Kinetics of Solute Partitioning into Ultrathin Nafion Films on Electrode Surfaces: Theory and Experimental Measurement

ARTICLE *in* THE JOURNAL OF PHYSICAL CHEMISTRY C · JANUARY 2007

Impact Factor: 4.77 · DOI: 10.1021/jp065398l

4 AUTHORS, INCLUDING:

Paolo Bertoncello
Swansea University
41 PUBLICATIONS **1,272** CITATIONS

SEE PROFILE

Kinetics of Solute Partitioning into Ultrathin Nafion Films on Electrode Surfaces: Theory and Experimental Measurement

Paolo Bertoncello,*,† Ilenia Ciani,† Davide Marenduzzo,‡ and Patrick R. Unwin*,†

Department of Chemistry, University of Warwick, Coventry CV4 7AL, United Kingdom and School of Physics, University of Edinburgh, Edinburgh EH9 3JZ, United Kingdom

Received: August 21, 2006; In Final Form: October 16, 2006

A simple voltammetric procedure for measuring the kinetics of slow partitioning processes into thin films is described and applied to determine the transport of trimethylammonium ferrocinium, FA^+, into ultrathin Nafion Langmuir−Schaefer films. By recording cyclic voltammograms for the oxidation of FA^+ as a function of time of a Nafion modified electrode placed in a dilute solution containing FA^+, one can readily measure the uptake of FA^+ into a film. An analytical model for the charge accumulated in the film has been derived for the cases of (i) transport-controlled partitioning; (ii) transport with a kinetic barrier at the film/solution (f/s) interface; and (iii) pure kinetic control. Analysis of experimental data indicates that, in contrast to dropcast Nafion films, there is a significant kinetic barrier at the f/s interface to FA^+ partitioning. The methodology and theory described are generic and could be applied to other chemical systems and detection methods.

Introduction

Nafion is one of the most common membrane materials used in polymer electrolyte fuel cells and has been the subject of extensive investigations since the 1970s.[1−5] Current applications of Nafion membranes include its use as a membrane separator in fuel cells,[6,7] batteries,[8,9] and water electrolizers.[10,11] Nafion is a polymer comprising a polytetrafluoroethylene-like backbone and perfluorinated side chains with terminating sulfonic acid groups.[2] The perfluorination confers excellent chemical, thermal, and electrochemical stability, while the sulfonic acid groups provide superacidity properties[2] as well as very good ion-exchange and permselectivity characteristics.[12] These properties and the availability of Nafion as a hydroalcoholic solution have inspired electrochemists to utilize Nafion to modify electrode surfaces so as to produce chemically modified electrodes[12−15] and voltammetric sensors.[16−18]

In general, the practical applications of Nafion require a detailed understanding of the transport properties of water and ions within this material.[2,3,10] Measurements of ion transport, particularly of redox-active ions within Nafion films, have been extensive[19−28] given the implications for the operation of electrocatalytic and biosensing systems. Ion-exchange coefficients for electroactive cations have been evaluated, which show a preference of Nafion for hydrophobic cations.[29−31] White et al.[12] and Anson and co-workers[14,19,21,24−26] reported detailed investigations on the mechanisms of charge transport within Nafion-coated electrodes using voltammetric methods; they were able to evaluate the contributions of physical diffusion and electron hopping to the apparent diffusion coefficient of different organic cations.

In general, the transport properties of redox species within Nafion have been evaluated on macroelectrodes using films having thicknesses from hundreds of nanometers to a few micrometers via cyclic voltammetry[13,26,29−31] and chronoamperometry.[12,22,31,32] However, the rate of charge transport in Nafion film has also been investigated using ultramicroelectrodes[22] and scanning electrochemical microscopy (SECM) approaches.[33,34]

New procedures have recently been developed for obtaining ultrathin films of Nafion with thicknesses of the order of tens of nanometers: Heineman[35] and Seliskar[36] fabricated Nafion films using a spin coating, and recently, one of the authors developed a novel procedure based on the Langmuir−Schaefer (LS) technique.[37−40] The apparent diffusion coefficients for the $Ru[(bpy)_3]^{2+}$ (bpy = 2,2′-bipyridine) and trimethylammoniomethylferrocene (FA^+) incorporated within the latter type of the Nafion film which were determined using a novel SECM approach were in the range of 10^{-11} to 10^{-10} cm^2 s^{-1}.[40] These atypically low values of the apparent diffusion coefficients appear to be intrinsically linked to the LS technique which results in ordered molecular and polymeric film structures that show high compactness.[41]

In this paper, we report a detailed investigation of the partitioning properties of FA^+ into Nafion LS films using cyclic voltammetry. Analytical theory and a numerical model are developed to interpret the experimental data. An outcome of the studies herein is that there is a significant kinetic barrier to the partitioning process at the film/solution (f/s) interface, which is not apparent in studies of dropcast films where partitioning is generally assumed to be diffusion-limited.[12,30,36] The studies herein are of further significance because the preconcentration of cationic chromophores into ultrathin Nafion films has been proposed as an analytical procedure for trace-level detections;[35,36,42−44] clearly, knowledge of the partitioning kinetics is important for the effective application of these methods. Moreover, the theoretical treatment presented here is general, and the method could be applied to other thin film partitioning processes.

Theory

We consider the natural diffusion of an electroactive species (FA^+) from an infinitely thick solution into an ultrathin (tens

* Corresponding author. Phone: +44 (0) 2476 523264. Fax: +44 (0) 2476 524112. E-mail: p.r.unwin@warwick.ac.uk (P.R.U.); p.bertoncello@warwick.ac.uk (P.B.).

† University of Warwick.

‡ University of Edinburgh.

10.1021/jp065398l CCC: $37.00
Published on Web 12/02/2006

of nanometers thick) film on a substrate which is inert. We seek an expression for the amount of material within the film as a function of time in order to predict the saturation time which depends on a series of parameters which characterize the partitioning process. This problem can be solved analytically (at least with suitable approximation), and the analytical solution is sensitive to the critical parameters characterizing the system (e.g., film thickness, concentration of the electroactive species in solution, and the diffusion coefficients of the species of interest in the two phases).

The system under consideration is composed of two separated phases, the film and the solution. In each phase, mass transport is regulated by the diffusion equation in the direction perpendicular to the f/s interface:

$$\text{inside the film:} \quad \frac{\partial c_f(x,t)}{\partial t} = D_f \frac{\partial^2 c_f(x,t)}{\partial x^2} \tag{1}$$

$$\text{in solution:} \quad \frac{\partial c_s(x,t)}{\partial t} = D_s \frac{\partial^2 c_s(x,t)}{\partial x^2} \tag{2}$$

where c_f, D_f, c_s, and D_s are the concentrations and the diffusion coefficients within film (subscript f) and in the solution (subscript s), respectively. The x-coordinate is normal to the f/s interface, and by treating the problem in one dimension, we assume that the film is of sufficient area that diffusional edge effects are negligible. The implications of this approximation are considered herein.

If l is defined as the thickness of the film, then the initial conditions in both phases can be written as

$$0 < x < l \qquad c_f(x,0) = 0 \tag{3}$$

$$l < x < \infty \qquad c_s(x,0) = c_s^* \tag{4}$$

The system is semi-infinite in the solution phase, and there is no flux at the solid support on which the Nafion film is deposited. The compatibility of the latter condition with the measurements which follow are discussed (vide infra). This leads to the following boundary conditions:

$$\lim_{x\to\infty} c_s(x,t) = c_s^* \tag{5}$$

$$\frac{\partial c_f(0,t)}{\partial x} = 0 \tag{6}$$

Case 1: No Kinetic Barrier at the f/s Interface. In the simplest case, we consider a system where the extraction from the solution into the film occurs without any kinetic barrier, as reported for dropcast films.[12] Thus, at the f/s interface, the conditions define the continuity of flux of material and assume a rapid extraction (defined by an equilibrium constant, K) from the solution to the film:

$$D_f \left.\frac{\partial c_f(x,t)}{\partial x}\right|_{x=l} = D_s \left.\frac{\partial c_s(x,t)}{\partial x}\right|_{x=l} \tag{7}$$

$$c_f(l,t) = K c_s(l,t) \tag{8}$$

The description of the partitioning process as reversible is appropriate in light of earlier studies of FA^+ absorption into Nafion at the solution concentrations of interest.[12] The Laplace transformation of eqs 1 and 2 yields the general solutions

$$\begin{cases} \hat{c}_f(x,s) = A e^{-\sqrt{(s/D_m)}x} + B e^{\sqrt{s/D_f}x} \\ \hat{c}_s(x,s) = C e^{-\sqrt{(s/D_s)}x} + \dfrac{c_s^*}{s} \end{cases} \tag{9}$$

where $\hat{c}_f(x,s)$ and $\hat{c}_s(x,s)$ denote the Laplace transformations of $c_f(x,t)$ and $c_s(x,t)$, respectively.

By using the boundary condition in eq 6 we obtain $A = B$ in eq 9. Meanwhile, applying the conditions in eqs 7 and 8 to eq 9 yields a system with two equations and two unknown terms (the constants A and C), which can easily be solved. After some algebra, the Laplace transform of the concentration inside the film is found to be

$$\hat{c}_f = \frac{K c_s^*}{s} \frac{1}{1+\beta} \frac{e^{-\sqrt{(s/D_s)}(x+l)} + e^{\sqrt{(s/D_s)}(x-l)}}{1 - e^{-2\sqrt{(s/D_s)}l}\left(\dfrac{\beta-1}{\beta+1}\right)} \tag{10}$$

where $\beta = K\sqrt{(D_f/D_s)}$. Equation 10 can be expanded as a power series to give

$$\hat{c}_f = \frac{K c_s^*}{s} \frac{1}{1+\beta} \sum_{n=0}^{\infty} \left[\frac{e^{\sqrt{(s/D_s)}(x-l(2n+1))}}{s} + \frac{e^{-\sqrt{(s/D_s)}(x+l(2n+1))}}{s} \right] \left(\frac{\beta-1}{\beta+1}\right)^n \tag{11}$$

Finally, the inverse Laplace tranformation applied to eq 11 yields

$$c_f = \frac{K c_s^*}{1+\beta} \sum_{n=0}^{\infty} \left[\operatorname{erfc}\left(\frac{l(2n+1)-x}{2\sqrt{tD_f}}\right) + \operatorname{erfc}\left(\frac{l(2n+1)+x}{2\sqrt{tD_f}}\right) \right] \left(\frac{\beta-1}{\beta+1}\right)^n \tag{12}$$

The amount of material within the film can be obtained by integrating the concentration across the thickness of the film. Because we evaluate this quantity by coulometry (vide infra), we calculate the charge, Q:

$$nFA_e \int_0^l c_f(x,t)\, dx = Q \tag{13}$$

where n is the number of electrons transferred in the detection of the redox species, A_e is the electrode area, and F is Faraday's constant.

Equation 13 is solved through integration by parts, noting that

$$\frac{\partial \operatorname{erfc}(x)}{\partial x} = -\frac{2}{\sqrt{\pi}} e^{-x^2} \tag{14}$$

The final expression for the quantity Q is given by

$$Q = nFA\frac{Kc_s^*}{1+\beta}\sum_{n=0}^{\infty}\left(\frac{\beta-1}{\beta+1}\right)^n\left[l\,\mathrm{erfc}\left(\frac{(n+1)l}{\sqrt{D_s t}}\right)+ l\,\mathrm{erfc}\left(\frac{nl}{\sqrt{D_s t}}\right)-(2n+1)l\left(\mathrm{erf}\left(\frac{(n+1)l}{\sqrt{D_s t}}\right)-\mathrm{erf}\left(\frac{nl}{\sqrt{D_s t}}\right)\right)+ \frac{2\sqrt{D_s t}}{\sqrt{\pi}}\left(\mathrm{e}^{-\frac{n^2l^2}{D_s t}}-\mathrm{e}^{-\frac{(n+1)^2l^2}{D_s t}}\right)\right] \quad (15)$$

Typical Q versus t plots are given in Figure 1 to illustrate the effect of film thickness and K. In Figure 1a, K is fixed at a value of 25 000, and the film thickness is varied from 10 to 100 nm. It can be seen that the thinner the film, the quicker it saturates, as expected. Moreover, in the long time limit, Q is proportional to the film thickness, also as anticipated. In Figure 1b, a typical film thickness of 30 nm is considered, and as K varies from 500 to 50 000, it can be seen that the final quantity of material in the film increases proportionally. Furthermore, the greater the value of K, the longer the time required to achieve saturation of the film, as expected. The data in Figure 1 are for typical diffusion coefficients values, $D_s = 6 \times 10^{-6}$ cm^2 s^{-1} and $D_f = 9 \times 10^{-11}$ cm^2 s^{-1}.[12,40]

Case 2: Kinetic Barrier at the f/s Interface. When there is a kinetic limitation to partitioning at the f/s interface, the conditions at the interfacial boundary, in Laplace space, become

$$D_f\left.\frac{\partial \hat{c}_f(x,s)}{\partial x}\right|_{x=l} = D_s\left.\frac{\partial \hat{c}_s(x,s)}{\partial x}\right|_{x=l} \quad (16)$$

$$D_f\left.\frac{\partial \hat{c}_f(x,s)}{\partial x}\right|_{x=l} = -k(\hat{c}_f(l,s) - K\hat{c}_s(l,s)) \quad (17)$$

where k (m s^{-1}) is the rate constant for the transfer of material from the solution phase to the film, assuming first-order heterogeneous kinetics. Writing the loading process as reversible is consistent with previous studies of FA^+ partitioning into thick Nafion films.[12,22,30]

Using the conditions in eqs 16 and 17 to solve the system in eq 9 (with $A = B$), we find, as a result, the following equations:

$$\begin{cases} \sqrt{D_f}A(\mathrm{e}^{\sqrt{(s/D_f)}l} - \mathrm{e}^{-\sqrt{(s/D_f)}l}) = -C\sqrt{D_s}\mathrm{e}^{-\sqrt{(s/D_s)}l} \\ \sqrt{D_f}\sqrt{s}A(\mathrm{e}^{\sqrt{(s/D_f)}l} - \mathrm{e}^{-\sqrt{(s/D_f)}l}) = \\ -k\left[A(\mathrm{e}^{\sqrt{(s/D_f)}l} + \mathrm{e}^{-\sqrt{(s/D_f)}l}) - K\left(C\mathrm{e}^{\sqrt{(s/D_s)}l} + \frac{c_s^*}{s}\right)\right] \end{cases} \quad (18)$$

Solving the system for A and C, we find the concentration within the film can be written as follows:

$$\hat{c}_f(s,x) = \frac{Kc_s^*}{s(\beta+1)}\frac{\mathrm{e}^{-\sqrt{(s/D_s)}(l-x)} + \mathrm{e}^{-\sqrt{(s/D_s)}(l+x)}}{1 - \mathrm{e}^{-2\sqrt{(s/D_f)}l}\left(\frac{\beta-1}{\beta+1}\right) + \frac{\sqrt{s}\sqrt{D_f}}{k(\beta+1)}(1 - \mathrm{e}^{-2\sqrt{(s/D_f)}l})} \quad (19)$$

Integrating this quantity between 0 and l allows us to find the Laplace transform of $Q/(nFA)$:

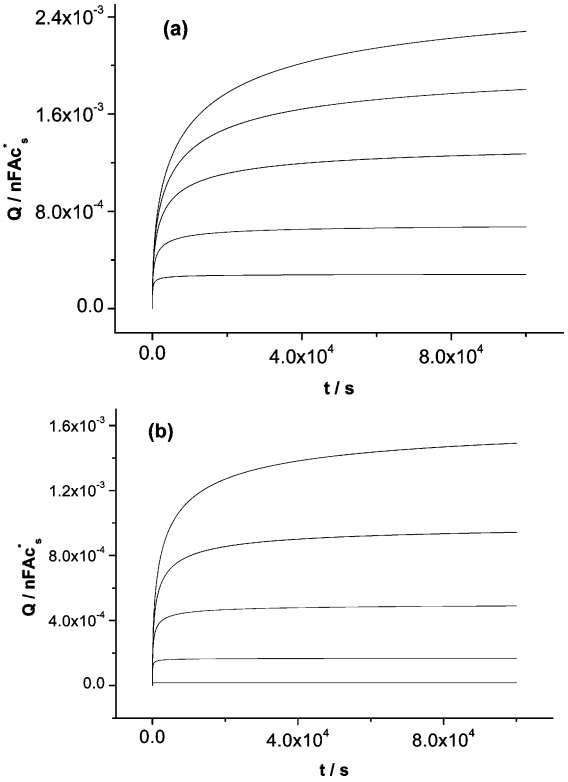

Figure 1. Q vs t plots obtained from eq 15 with $D_s = 6 \times 10^{-6}$ cm^2 s^{-1} and $D_f = 9 \times 10^{-11}$ cm^2 s^{-1}. (a) From bottom to top $l = 10$, 25, 50, 75, and 100 nm; $K = 25\,000$. (b) From bottom to top, $K = 500$, 5000, 15 000, 30 000, and 50 000 ($l = 30$ nm).

$$\frac{\hat{Q}}{nFA} = \frac{Kc_s^*}{s(\beta+1)}\frac{\int_0^{2l}\mathrm{e}^{-\sqrt{(s/D_f)}x}\,\mathrm{d}x}{(1 - \mathrm{e}^{-2\sqrt{(s/D_f)}l})\frac{\sqrt{sD_f}}{k(\beta+1)} + 1 - \frac{\beta-1}{\beta+1}\mathrm{e}^{-2\sqrt{(s/D_f)}l}} = \frac{\frac{Kc_s^*}{s(\beta+1)}}{\sqrt{D_f/s}\frac{(1 - \mathrm{e}^{-2\sqrt{(s/D_f)}l})}{1 - \frac{\beta-1}{\beta+1}\mathrm{e}^{-2\sqrt{(s/D_f)}l} + (1 - \mathrm{e}^{-2\sqrt{(s/D_f)}l})\frac{\sqrt{sD_f}}{k(\beta+1)}}} \quad (20)$$

To the best of our knowledge, Q cannot be found analytically, and it is necessary to perform some approximations. First, let us consider the limit for large s (corresponding to short times). In this case, we obtain the following asymptotic behavior for $\hat{Q}$:

$$\frac{\hat{Q}}{nFA} \underset{s\to+\infty}{\approx} \frac{Kkc_s^*}{s\sqrt{s}}\frac{1}{k(K\sqrt{(1/D_s)} + \sqrt{(1/D_f)}) + \sqrt{s}} \quad (21)$$

It is now possible to calculate the Laplace anti-transform of eq 21, knowing that[46]

$$L^{-1}\left(\frac{1}{s}\right) = 1$$
$$L^{-1}\left(\frac{1}{\sqrt{s}}\frac{1}{a+\sqrt{s}}\right) = \mathrm{e}^{a^2t}\,\mathrm{erfc}(at^{1/2}) \quad (22)$$

The convolution of the two Laplace anti-transforms (denoted

by L^{-1}) yields

$$L^{-1}\left(\frac{1}{s\sqrt{s}}\frac{1}{a+\sqrt{s}}\right) = \int_0^t e^{a^2\tau}\,\mathrm{erfc}(a\tau^{1/2})\,d\tau = \frac{1}{a^2}(e^{a^2t}\,\mathrm{erfc}(at^{1/2}) - 1) + \frac{2}{a^2\sqrt{\pi}}\int_0^t \frac{e^{a^2\tau}e^{-a^2\tau}a}{2\sqrt{\tau}}d\tau = \frac{1}{a^2}(e^{a^2t}\,\mathrm{erfc}(at^{1/2}) - 1) + \frac{2\sqrt{t}}{a\sqrt{\pi}} \quad (23)$$

Thus, for large s, the charge, Q, within the film is given by

$$Q(t) = nFAKkc_s^*\left[\frac{1}{\gamma^2}(e^{\gamma^2t}\,\mathrm{erfc}(\gamma t^{1/2}) - 1) + \frac{2\sqrt{t}}{\gamma\sqrt{\pi}}\right] \quad (24)$$

where

$$\gamma = k(K\sqrt{(1/D_s)} + \sqrt{(1/D_f)}) \quad (25)$$

It is interesting to note that for $t \rightarrow 0$, $Q(t)$ is linear with t and depends only on K and k (not on the diffusion coefficients or the film thickness):

$$Q(t) \underset{t\rightarrow 0}{\approx} nFAKkc_s^*t \quad (26)$$

Using the limiting behavior of eq 20 for $s \rightarrow 0$ and performing the Laplace inverse transform of that limit for large times, we obtain

$$Q(t) \underset{t\rightarrow \infty}{=} nFAKc_s^*l \quad (27)$$

As we now have the correct behavior of the function $Q(t)$ for 0, small, and large times, we may use a family of interpolating functions to describe the $Q(t)-t$ curves for all times:

$$Q(t) = nFAKc_s^*l\left\{\tanh\left[\frac{k}{l}\left(\frac{1}{\gamma^2}(e^{\gamma^2t}\,\mathrm{erfc}(\gamma t^{1/2}) - 1) - \frac{2\sqrt{t}}{\gamma\sqrt{\pi}}\right)\right]^\alpha\right\}^{1/\alpha} \quad (28)$$

We note that all positive values of α yield the correct asymptotic behavior for small and large times. To find the optimal value of α, we solved eqs 1 and 2, subject to the boundary conditions in eqs 3−6 and in eqs 16−17, using the FemLab−Matlab package. Fitting eq 28 to the numerical data suggested that $\alpha = 0.5$ fitted the data most precisely for the range of experimental conditions encountered in the studies herein.

To illustrate the effect of interfacial kinetics, plots of Q versus t (for the case of $l = 30$ nm) are reported in Figure 2 for different values of k. From 1×10^{-8} to 5×10^{-10} cm s^{-1}, the data indicate a strong dependence of the $Q-t$ curves on k; these data indicate that it should be possible to readily elucidate kinetic constants for interfacial transfer over this range.

The approach described is, of course, only sensitive to slow interfacial kinetics because of the inherently low diffusion rates in this type of experiment. This is evident from Figure 3, which shows simulated concentration profiles inside and outside of a 30 nm thick film (from the numerical model) at different times with (a) no kinetic barrier and (b) $k = 10^{-9}$ cm s^{-1}. As above, $D_s = 6 \times 10^{-6}$ cm^2 s^{-1} and $D_f = 9 \times 10^{-11}$ cm^2 s^{-1} were used in the simulation, with $K = 2.5 \times 10^4$. The profiles inside the film are seen to be flat and indicate that the film concentration increases with time. The flat concentration profile is expected

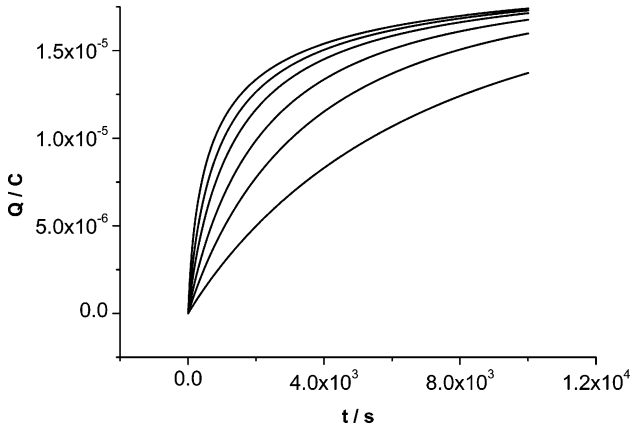

Figure 2. Q vs t plots obtained from the analytical expressions in eqs 28 and 25. $D_s = 6 \times 10^{-6}$ cm^2 s^{-1} and $D_f = 9 \times 10^{-11}$ cm^2 s^{-1}, $K = 25\,000$, $l = 30$ nm, and $\alpha = 0.5$. From top to bottom, $k = 1 \times 10^{-8}$, 5×10^{-9}, 3×10^{-9}, 1.7×10^{-9}, 1×10^{-9}, and 5×10^{-10} cm s^{-1}.

in view of the very small film thickness: it takes less than 0.1 s for a molecule to diffuse across the whole film, even though the diffusion coefficient in the film is small. Significant concentration gradients are apparent in the solution. Note that the x axis range in Figure 3a,b has been reduced for clarity: in the simulations, it was set to 0.3 m to ensure the complete restoration of the bulk concentration even at the largest time. By comparing Figure 3a,b, we see that the effect of the kinetics (in Figure 3b) leads to a higher concentration of species at the f/s interface because the flux of species into the film is reduced (compare, for example, the data after 100 s, where the concentration is ca. 0.0014 mol m^{-3} in Figure 3a but 0.0072 mol m^{-3} in Figure 3b). As time progresses, there is an increased depletion zone which extends further from the interface, and the profiles for the two cases become more similar. This is because, at larger times, the mass transport rate becomes very low indeed and so tends to become the limiting step. Moreover, at larger times, the equilibrium situation is approached. Indeed, at 10^7 s, essentially flat profiles, close to bulk, result in solution for both cases because the film reaches equilibrium.

In practice, one needs to consider the validity of describing mass transport in terms of diffusion over extended time and lengths and the implications for the analysis of experimental data. It follows from Figures 1−3 that, for the typical conditions of the experiments described herein, the approximate diffusion layer thickness is smaller than the electrode dimension (approximately 5 mm) for $t \leq 10^4$ s. For the studies herein, this time scale is sufficient for complete saturation, and so the assumption of planar diffusion (with negligible edge effects) is reasonable. On large time scales, natural convection will also tend to be more important. However, the experiments are carried out with only trace concentrations in the aqueous phase, and so density gradients will be negligible. Furthermore, experiments were carried out in a completely enclosed environment on a vibrational isolation bench to minimize external effects. Moreover, the theory presented indicates that kinetics will be most apparent at short times where complications of the type mentioned are less likely. Since the effect of natural convection would be to enhance transfer rates in solution and thus partitioning kinetics, the next section considers the situation where there is no concentration gradient in solution, as an extreme limiting kinetic case.

Case 3: Kinetic Barrier at the f/s Interface with Fixed Concentration in Solution. We now consider the same problem as above but where the concentration in solution remains constant; that is, transport in solution is not a factor. This is an

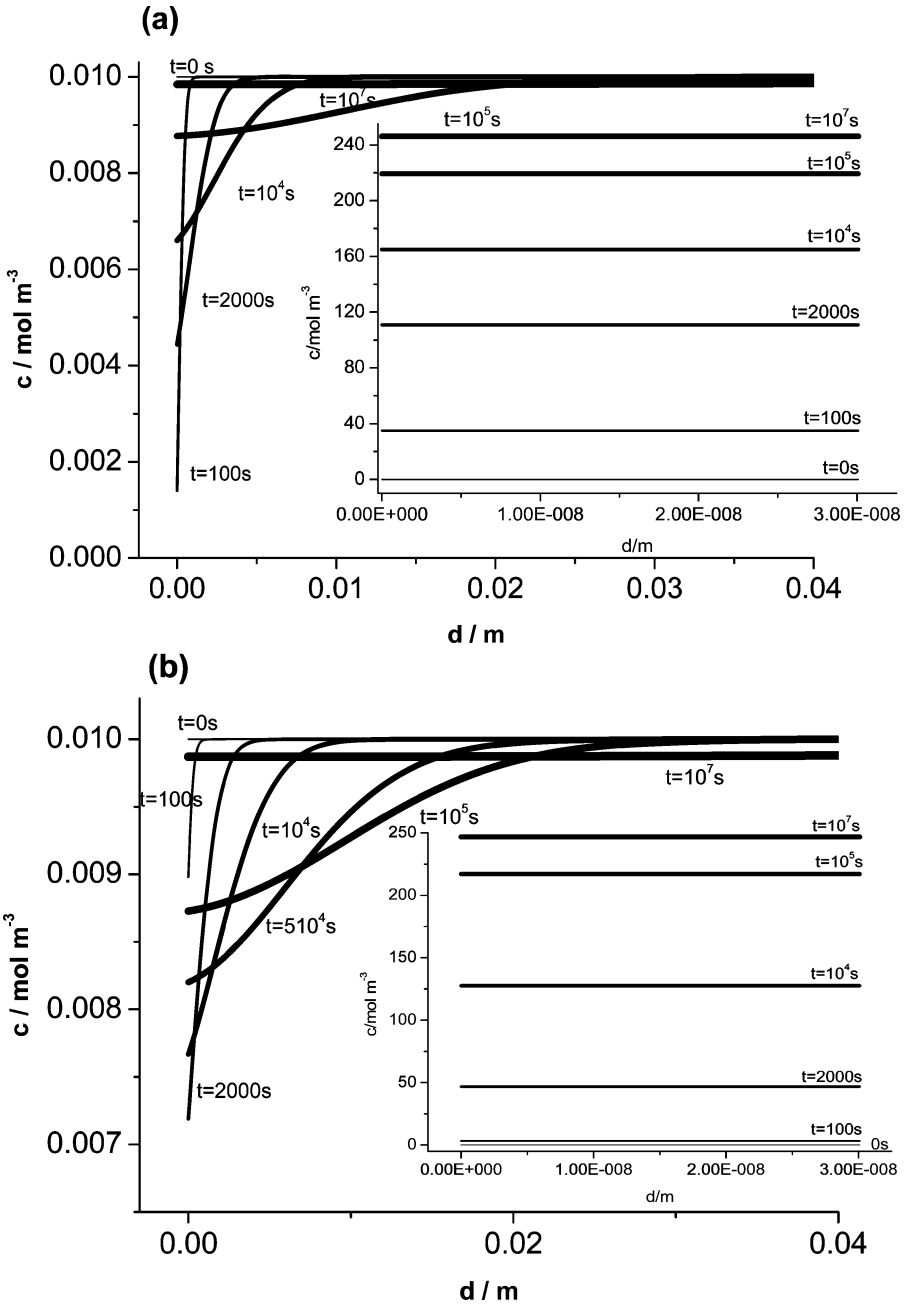

Figure 3. Simulated concentration profiles adjacent to a thin film ($l = 30$ nm) at different times. The insets represent the corresponding concentration profiles inside the film which are seen to be flat. Values of $D_s = 6 \times 10^{-6}$ cm^2 s^{-1}, $D_f = 9 \times 10^{-11}$ cm^2 s^{-1}, and $K = 2.5 \times 10^4$ were used with (a) no kinetic barrier and (b) $k = 10^{-9}$cm s^{-1}.

interesting case as it allows one to estimate the maximum rate at which a film can saturate (under complete kinetic control). This means that the problem is now reduced to the consideration of a single phase, so the boundary condition in eq 17 in (x,t) space becomes

$$D_f \left.\frac{\partial c_f(x,t)}{\partial x}\right|_{x=l} = -k(c_f(l,t) - Kc_s^*) \qquad (29)$$

This problem can be analyzed using the same analytical techniques described, and the solution is given by eq 28 with

$$\gamma = k\sqrt{(1/D_f)} \qquad (30)$$

Indeed, the assumption that the concentration in solution remains constant is equivalent to calculating the limiting solution of the problem considered above for $D_s \rightarrow \infty$. This was confirmed by fitting the simulated data obtained with eq 29, rather than eq 17, with the analytical model. We note that in this case the numerical data were better fitted using $\alpha = 0.7$ in eq 28 with γ given by eq 30. This case is considered further in conjuction with the experimental data discussed later.

Experimental Section

Materials. Nafion 117 solution (5% w/v mixture of low molecular weight alcohols), NaCl, and all other chemicals were purchased from Aldrich and used as received. $FA^+(Cp_2FeTMA^+)PF_6^-$ was obtained from metathesis of FA^+ iodide with $AgPF_6$.[30] The electrochemical experiments were carried out using indium−tin−oxide (ITO) glass plates from Delta Technologies, Ltd. (U.S.A.), with resistivity, $R_s \leq 10$ Ω/sq, as the working electrode for the deposition of Nafion. Before use, ITO glass plates were sonicated in isopropanol, acetone, and chloroform for at least 5

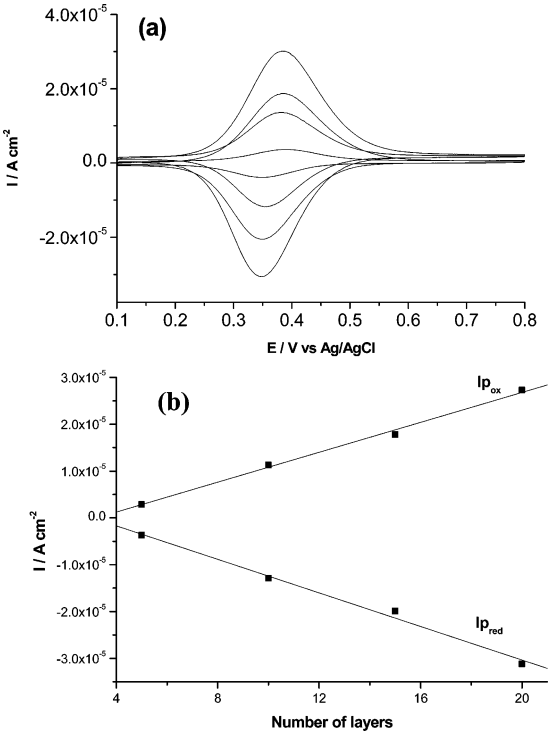

Figure 4. CVs (scan rate 20 mV s^{-1}) of 5-, 10-, 15-, and 20-layer (from bottom to top) Nafion LS films loaded to a limit from 5×10^{-4} M FA^+, after transferring to 0.1 M NaCl supporting electrolyte (a). Anodic and cathodic peak current density vs number of layers (b).

min. The substrates were then dried using nitrogen gas. Before use, the substrates were cleaned with chloroform. All aqueous solutions were prepared from doubly distilled Milli-Q reagent water (Millipore Corp.) with a resistivity ≥18.2 MΩ cm at 25 °C.

Methods. *Electrochemistry.* Cyclic voltammograms (CVs) and chronoamperometry characteristics were recorded using an electrochemical analyzer (CH Instruments, model CHI730A). A conventional three-electrode configuration was used, where the working electrode was an ITO glass plate on which a Nafion LS film had been deposited; a platinum coil was used as a counter electrode and either a Ag/AgCl or a KCl saturated calomel electrode was used as reference electrodes. The area of the working (typically between 0.2 and 0.3 cm^2) electrode was kept constant during all measurements.

Fabrication of Nafion LS Films. Nafion LS films were fabricated using a well-established procedure described in literature.[37,45] Briefly, a stock solution of Nafion was prepared by dilution of the commercial solution with methanol to obtain a final concentration of 0.85 mg/mL. Nafion Langmuir monolayers were formed using a Langmuir trough (Nima Instruments, Coventry, U.K.). The surface pressure was measured by means of a Wilhelmy balance with an accuracy of ±0.1 mN m^{-1}. The volume of Nafion added to the surface of the aqueous subphase (0.1 m NaCl) varied between 100 and 200 μL. A period of 2 min was allowed to elapse before compression of the floating film. On the basis of the Langmuir isotherm, a surface pressure of 20 mN m^{-1} was employed for LS deposition.[37,40]

Results and Discussion

Voltammetry of Nafion LS Films. We use voltammetry to measure the dynamics of partitioning into Nafion LS films, and so first consider the voltammetric response of films preloaded with FA^+. Figure 4 reports the CVs (scan rate 20 mV s^{-1}) of 5-, 10-, 15-, and 20-layer Nafion LS films, first loaded to saturation from 0.5 mM FA^+ and then transferred to a solution containing only supporting electrolyte. The anodic and cathodic peak potentials for the one-electron oxidation of FA^+ and reduction of the product are respectively $E_p^a = 0.38$ V and $E_p^c = 0.34$ V (vs Ag/AgCl; $\Delta E_p = E_p^a - E_p^c = 40$ mV).[46] The CV is reasonably characteristic of a surface-confined redox process,[46] particularly as ΔE_p was scan-rate-dependent, decreasing to 20 mV at a scan rate of 5 mV s^{-1} (data not shown). Moreover, at a low scan rate, the anodic and cathodic peak currents scaled linearly with the number of layers (see Figure 4b). The concentration of FA^+ incorporated into the Nafion films was calculated from thickness measurements, and the charge, Q, was consumed for the complete oxidation of FA^+.[40] Film thickness information was obtained using atomic force microscopy (AFM), as outlined in detail elsewhere.[40] The LS films were found to have a thickness of 1.4 ± 0.1 nm per layer before loading and 1.7 ± 0.1 nm per layer after loading in FA^+.

Figure 5 shows a set of CVs of a typical 30-layer film loaded to saturation in 10^{-5} M FA^+, after transferring to a solution containing only 0.1 M NaCl supporting electrolyte. Figure 5b, the anodic peak currents versus the scan rate (10−500 mV s^{-1}), reveals a linear dependence for low scan rate, while at the higher scan rates, the plot of the anodic peak currents tends to scale more linearly with the square root of the scan rate (data not shown). The latter behavior is indicative of a switch toward a diffusion-controlled system.[46] Further confirmation of the switch between thin layer behavior and semi-infinite diffusion (as the scan rate increases) can be seen in Figure 5b, which shows Q on the anodic sweep as a function of the scan rate. At low scan rates (υ < 10 mV s^{-1}), exhaustive electrolysis is evident, but as the scan rate increases, Q decreases.

Dynamics of FA^+ Transfer into Nafion LS Films. In order to investigate the dynamics of FA^+ transfer to Nafion LS films, aqueous dilute solutions were used. Figure 6 shows CVs of a 30-layer Nafion LS film during loading from aqueous 10^{-5} M FA^+ (0.1 M NaCl) under quiescent solution conditions. For clarity, we report only the first 100 cycles. It can be seen that as the time increases, the magnitude of the current response increases because of the time-dependent incorporation of FA^+ into the film. The scan rate for these studies was 0.1 V s^{-1}, which ensured good time resolution. At this scan speed, a sizable fraction of the charge in the film is measured during a CV scan, but it was necessary to use data, such as those in Figure 5, obtained on fully loaded (saturated) films to calibrate the fraction of the total charge detected. On the time scale of a voltammetric scan, the diffusion layer induced by the electroanalytical process extends from the electrode slightly beyond the f/s boundary, and it is important to consider the effect on the measurement methodology. Significantly, at relatively short to moderate times (low loading levels), the voltammetric consumption of FA^+ in the film is expected to have only a negligible effect on the partitioning process because it is far from equilibrium and driven in the direction of transfer to the film with negligible back transfer (see, e.g., eq 17). As outlined above, it is this portion of the $Q-t$ data which is most sensitive to interfacial kinetics.

We first consider the analysis of $Q-t$ data in terms of eq 15 which assumes no interfacial kinetic barrier. Figure 7 shows experimental data for three different Nafion films: 20, 30, and 40 layers. To fit the curves, the following parameters must be known: D_s, D_f, l, and K. The diffusion coefficients of FA^+ in solution and inside the film are established, and their values are $D_s = 6 \times 10^{-6}$ cm^2 s^{-1} [40] and $D_f = 9 \times 10^{-11}$ cm^2 s^{-1},[12,40] respectively, although as evident from the concentration profiles

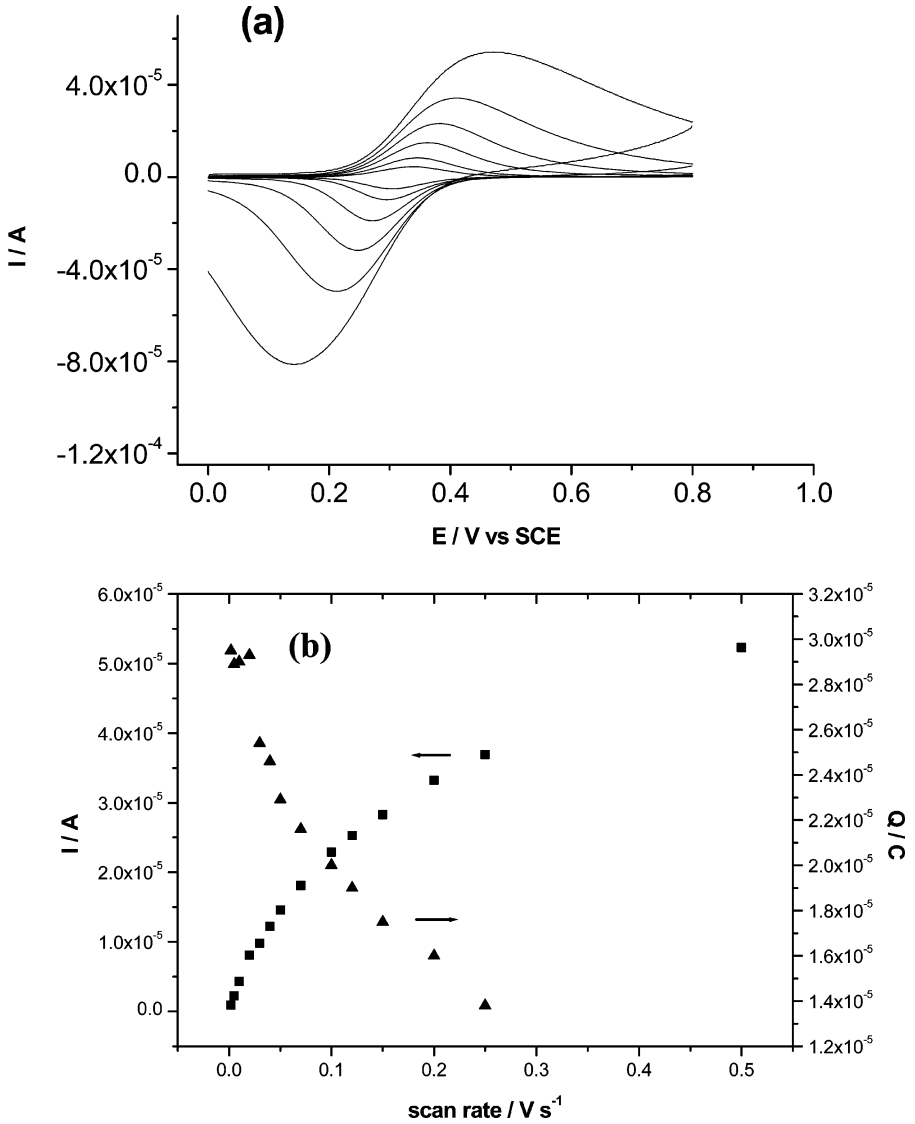

Figure 5. CVs of a 30-layer Nafion LS film loaded to a limit from 10^{-5} M FA^+ and then transferred to 0.1 M NaCl supporting electrolyte. (a) Scan rates are 10, 20, 50, 100, 200, and 500 mV s^{-1} (from bottom to top). (b) Anodic peak current (■) and charge (▲) vs scan rate.

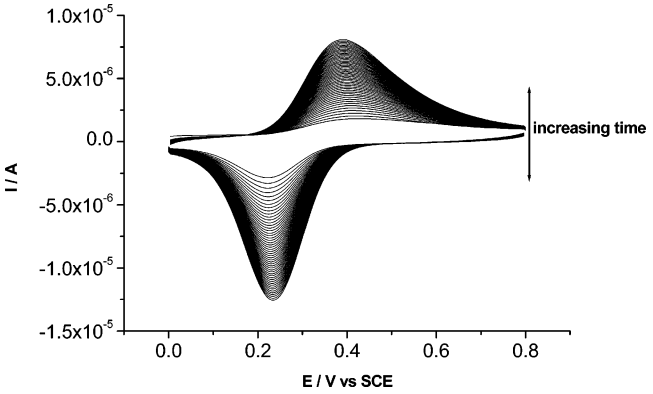

Figure 6. CVs of a 30-layer Nafion LS film during loading from 10^{-5} M FA^+. Scan rate of 100 mV s^{-1}, supporting electrolyte 0.1 M NaCl. For clarity, only the first 100 cycles are shown.

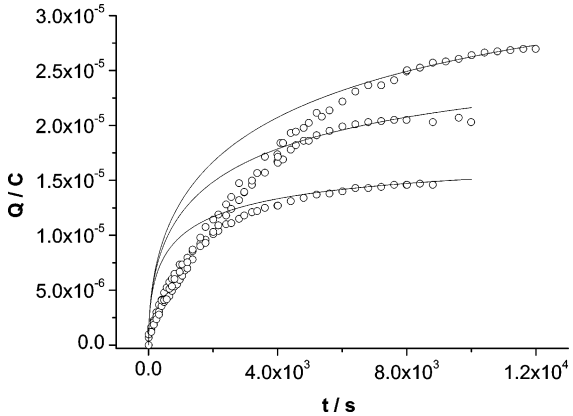

Figure 7. Experimental (○) and analytical theory (lines) from eq 15 for Q vs t during the partitioning of FA^+ from a 10^{-5} M solution. From top to bottom, data are for films: 40 layers, $l = 65$ nm; 30 layers, $l = 46$ nm; 20 layers, $l = 27$ nm; and $K = 3.6 \times 10^4$.

in Figure 3, the D_f value is non-limiting and, of this order, does not influence the simulations. AFM allowed the film thickness to be determined while K was obtained either by coulometry at the end of an experiment or by the fitting of the long time data obtained as the partitioning process approached equilibrium.

The agreement between theoretical and experimental data is only good for long times. At short to intermediate times, the experimental data lie below theory, indicating that there is a kinetic barrier to partitioning. Note that if there were any effects from natural convection then this would enhance Q in the time-dependent part of the $Q-t$ profiles. Thus, the data in Figure 7 clearly indicate an interfacial kinetic effect. It is interesting to

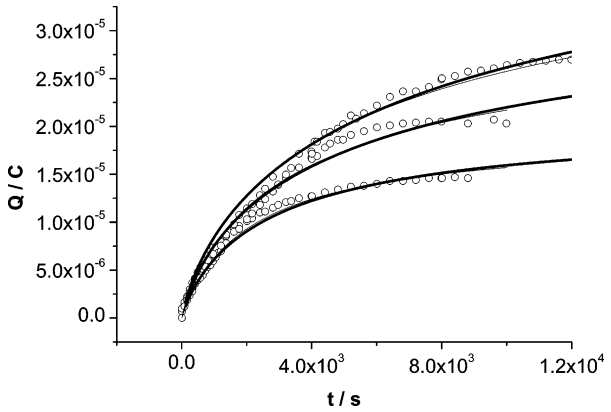

Figure 8. Experimental (○) and analytical expression (thick lines) from eqs 28 and 25 and numerically simulated data (thin lines) for Q vs t. $D_s = 6 \times 10^{-6}$ cm^2 s^{-1} and $D_f = 9 \times 10^{-11}$ cm^2 s^{-1}; $K = 3.6 \times 10^4$ and $\alpha = 0.5$. From top to bottom: 40 layers, $l = 65$ nm, $k = 2.7 \times 10^{-9}$ cm s^{-1}; 30 layers, $l = 46$ nm, $k = 2.3 \times 10^{-9}$ cm s^{-1}; and 20 layers, $l = 27$ nm, $k = 1.7 \times 10^{-9}$ cm s^{-1}.

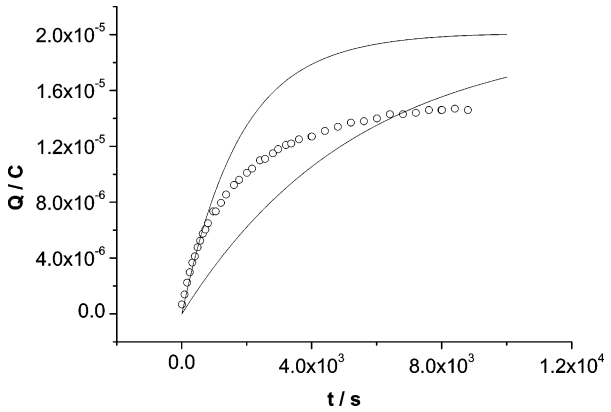

Figure 9. Experimental (○) and analytical expression (lines) from eq 28 with the condition in eq 30, for Q vs t for a 20-layer film, with $l = 27$ nm, $D_s = 6 \times 10^{-6}$ cm^2 s^{-1}, $D_f = 9 \times 10^{-11}$ cm^2 s^{-1}, and $\alpha = 0.7$, $K = 3.6 \times 10^4$. The top curve is for $k = 1.5 \times 10^{-9}$ cm s^{-1} while the bottom curve is for $k = 5 \times 10^{-10}$ cm s^{-1}.

note that a recent study of FA^+ into micropores filled with Nafion suggested the presence of an interfacial kinetic barrier although the rate constant was not calculated.[47]

By introducing a kinetic barrier, a significantly better fit of the experimental data to the model (both analytical theory and simulations throughout the whole time scale considered; see Figure 8) was obtained. The fit between the theoretical and the experimental data allowed us to determine the value of the kinetic constant, k. The best fit of the experimental data was obtained for values of $k = 2.2 \pm 0.5 \times 10^{-9}$ cm s^{-1}. The low rate constant for partitioning is not surprising taking into consideration the high compactness of the LS films,[2,3,37] which also significantly impacts the diffusion coefficient within the films.[37−40] It is widely accepted that Nafion has a multiphase structure with hydrophobic regions (fluorocarbon backbone), hydrophilic ionic clusters (sulfonated groups), and interfacial regions.[2,3,5] In addition, Anson et al. demonstrated the presence in polymeric films of "Donnan domains" in which most of the ions are located and charge transport occurs.[50−52] The high compactness and rigidity introduced in the Nafion structure using the LS technique may make these features more prominent and contribute to the observed kinetic barrier.

To examine the possible influence of natural convection, which would tend to increase the concentration in the solution phase adjacent to the Nafion film, the experimental data were fitted with eq 28 by using the coefficient γ, given in eq 30, and $\alpha = 0.7$. An example of this analysis is shown in Figure 9 for the film with $l = 27$ nm. The data have been fitted to theory which approximates best to the behavior at short ($k = 1.5 \times 10^{-9}$ cm s^{-1}) and long ($k = 5 \times 10^{-10}$ cm s^{-1}) times. Encouragingly, at short times ($t < 800$ s), the simple surface-limited kinetic model fits the data well, with a rate constant only slightly lower than determined with the full model. This would be expected as, on this time scale, there is only a small depletion of the solution adjacent to the film. However, at longer times, the surface-limited analysis with this rate constant predicts higher Q than measured experimentally because the neglect of depletion in solution becomes a serious problem. By using a smaller rate constant ($k = 5 \times 10^{-10}$ cm s^{-1}), one can only poorly approximate the data at long times, and the analysis at the shorter times is particularly inadequate.

To eliminate concentration boundary layers in transport measurements, one can introduce stirring.[29,30,34,48,49] Figure 10 shows typical voltammetric data for a 30-layer film (10^{-5} M FA^+ in solution) as a function of time. In all, 250 cycles are shown (0.1 V s^{-1}), but a limiting response was achieved after only 4 min (15 cycles). This time scale should be compared with that observed experimentally in quiescent solution and, indeed, predicted under the surface-limited model where the solution concentration boundary layer is eliminated (10^4 s). The rapid uptake of FA^+ in the Nafion LS film with stirring indicates not only that mass transport in solution is increased but that there is also a significant impact on the kinetics of the process. Thus, the physicochemical properties of the film itself are significantly affected by stirring.

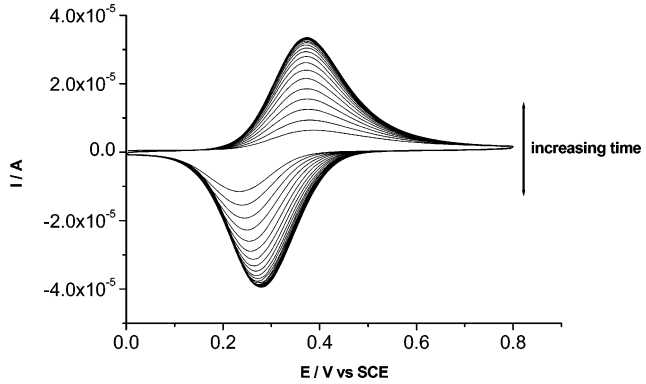

Figure 10. CVs of a 30-layer Nafion LS film during loading in 10^{-5} M FA^+ under stirred solution conditions. A total of 250 CVs are shown (scan rate 100 mV s^{-1}).

Conclusions

We have used a simple voltammetric procedure to measure the kinetics of FA^+ partitioning into ultrathin films of Nafion, fabricated using the LS technique. Different analytical models for the charge accumulated in the film as a function of time during loading have been derived and solved for three situations: (i) transport-controlled partitioning; (ii) transport with a kinetic barrier at the f/s interface; and (iii) pure kinetic control. Analysis of experimental data indicates that, in contrast to dropcast Nafion films, there is a significant kinetic barrier to FA^+ partitioning into Nafion LS films. This can be rationalized in terms of the more compact nature of these films, which also significantly impacts the diffusion coefficients in the films.[37,40]

The model developed is generic and could be applied to other slow thin-film partitioning processes. Moreover, although electrochemical analysis has been considered, the model was

formulated for a film on an inert substrate and so could be used to analyze partitioning data obtained by other methods, such as the quartz crystal microbalance or spectroscopy.

Acknowledgment. This research was supported by Marie Curie Intra-European Fellowships (P.B. fellowship, MEIF-CT-2005-515356, and I.C. fellowship, MEIF-CT-2004-501300) within the 6th European Community Framework Programme. D.M. acknowledges SUPA for support.

References and Notes

(1) Kordesch, K.; Simader, G. *Fuel Cells and their Applications*; VCH: Weinheim, Germany, 1996.
(2) *Perfluorinated Ionomer Membranes*; Eisenberg, A., Yeager, H. L., Eds.; ACS Symposium Series 180; American Chemical Society: Washington, DC, 1982.
(3) Mauritz, K. A.; Hora, C. J.; Hopfinger, A. J. Theoretical Model for the Structures of Ionomers: Application to Nafion Materials. In *Ions in Polymers*; Eisenber, A., Ed.; Advances in Chemistry Series 187; American Chemical Society: Washington, DC, 1980; pp 123−144.
(4) Mauritz, K. A.; Moore, R. B. *Chem. Rev.* **2004**, *104*, 4535.
(5) Heitner-Wirguin, C. *J. Membr. Sci.* **1996**, *120*, 1.
(6) Tazi, B.; Savadogo, O. *Electrochim. Acta.* **2000**, *45*, 4329.
(7) Xing, B.; Savadogo, O. *Electrochem. Commun.* **2000**, *2*, 697.
(8) Will, F. G. *J. Electrochem. Soc.* **1979**, *126*, 35.
(9) Yeo, R. S.; Chin, D. T. *J. Electrochem. Soc.* **1980**, *10*, 741.
(10) Cutler, S. G. In *Ions in Polymers*; Eisenberg, A., Ed.; American Chemical Society: Washington, DC, 1980; Chapter 9.
(11) Pillai, K. C.; Kumar, A. S.; Zen, J.-M. *J. Mol. Catal. A* **2000**, *160*, 277.
(12) White, H. S.; Leddy, J.; Bard, A. J. *J. Am. Chem. Soc.* **1982**, *104*, 4811.
(13) Leddy, J.; Bard, A. J. *J. Electroanal. Chem.* **1985**, *189*, 203.
(14) Buttry, D. A.; Anson, F. C. *J. Am. Chem. Soc.* **1982**, *104*, 4824.
(15) Martin, C. R.; Rubinstein, I.; Bard, A. J. *J. Am. Chem. Soc.* **1982**, *104*, 4817.
(16) Ugo, P.; Moretto, L. M.; Vezzá, F. *ChemPhysChem* **2002**, *3*, 917.
(17) Gerardi, R. D.; Barnett, N. W.; Lewis, S. W. *Anal. Chim. Acta* **1999**, *378*, 1.
(18) Brett, C. M. A.; Fungaro, D. A.; Morgado, J. M.; Gil, M. H. *J. Electroanal. Chem.* **1999**, *468*, 26.
(19) Buttry, D. A.; Anson, F. C. *J. Am. Chem. Soc.* **1983**, *105*, 685.
(20) Murray, R. W. In *Electroanalytical Chemistry*; Bard, A. J., Ed.; M. Dekker: New York, 1984; Vol. 13, pp 191−368.
(21) Buttry, D. A.; Saveant, J. M.; Anson, F. C. *J. Phys. Chem.* **1984**, *88*, 3086.
(22) Whiteley, L. D.; Martin, C. R. *J. Phys. Chem.* **1989**, *93*, 4650.
(23) Blauch, D. N.; Saveant, J. M. *J. Am. Chem. Soc.* **1992**, *114*, 3323.
(24) Anson, F. C.; Blauch, D. N.; Saveant, J. M.; Shu, C.-F. *J. Am. Chem. Soc.* **1991**, *113*, 1922.
(25) Lee, C.; Anson, F. C. *Anal. Chem.* **1992**, *64*, 528.
(26) Shi, M.; Anson, F. C. *Langmuir* **1996**, *12*, 2068.
(27) Arkoub, I. A.; Amatore, C.; Sella, C.; Thouin, L.; Warcocz, J.-S. *J. Phys. Chem. B* **2001**, *105*, 8694.
(28) Yagi, M.; Sato, T. *J. Phys. Chem. B* **2003**, *107*, 4975.
(29) Martin, C. R.; Rubinstein, I.; Bard, A. J. *J. Am. Chem. Soc.* **1982**, *104*, 4817.
(30) Szentirmay, M. N.; Martin, C. R. *Anal. Chem.* **1984**, *56*, 1898.
(31) Shi, M.; Anson, F. C. *Anal. Chem.* **1997**, *69*, 2653.
(32) Martin, C. R.; Dollard, K. A. *J. Electroanal. Chem.* **1983**, *159*, 127.
(33) Mirkin, M. V.; Fan, F.-R. F.; Bard, A. J. *Science* **1992**, *257*, 364.
(34) Bath, B. D.; White, H. S.; Scott, E. R. *Anal. Chem.* **2000**, *72*, 433
(35) Andria, S. E.; Richardson, J. N.; Kaval, N.; Zudans, I.; Seliskar, C. J.; Heineman, W. R. *Anal. Chem.* **2004**, *76*, 3139.
(36) Pantelic, N.; Wansapura, C. M.; Heineman, W. R.; Seliskar, C. J. *J. Phys. Chem. B* **2005**, *109*, 13971.
(37) Bertoncello, P.; Ram, M. K.; Notargiacomo, A.; Ugo, P.; Nicolini, C. *Phys. Chem. Chem. Phys.* **2002**, *4*, 4036.
(38) Bertoncello, P.; Ugo, P. *J. Braz. Chem. Soc.* **2003**, *14*, 517.
(39) Ugo, P.; Bertoncello, P.; Vezzá, F. *Electrochim. Acta.* **2004**, *49*, 3785.
(40) Bertoncello, P.; Ciani, I.; Li, F.; Unwin, P. R. *Langmuir*, published online Aug 23, http://dx.doi.org/10.1021/la061214i.
(41) Petty, M. *Langmuir-Blodgett Films*; Cambridge University Press: Cambridge, U.K., 1996.
(42) Rubinstein, I.; Bard, A. J. *J. Am. Chem. Soc.* **1980**, *102*, 6641.
(43) Rubinstein, I.; Bard, A. J. *J. Am. Chem. Soc.* **1980**, *103*, 5007.
(44) Downey, T. M.; Nieman, T. A. *Anal. Chem.* **1992**, *64*, 261.
(45) Bertoncello, P.; Notargiacomo, A.; Nicolini, C. *Langmuir* **2005**, *21*, 172.
(46) Bard, A. J; Faulkner L. R. In *Electrochemical Methods: Fundamentals and Applications*, 2nd ed.; Wiley: New York, 2001.
(47) Uitto, O. D.; White, H. S.; Aoki, K. *Anal. Chem.* **2002**, *74*, 4577.
(48) Shou, C.-F.; Anson, F. C. *J. Phys. Chem.* **1990**, *94*, 8345.
(49) Tsou, Y.-M.; Anson, F. C.; *J. Phys. Chem.* **1995**, *89*, 3818.
(50) Anson, F. C.; Saveant, J.-M.; Shigehara, K. *J. Am. Chem. Soc.* **1983**, *105*, 1096.
(51) Inoue, T.; Anson, F. C. *J. Phys. Chem.* **1987**, *91*, 1519.
(52) Anson, F. C.; Ohsaka, T.; Saveant, J.-M. *J. Phys. Chem.* **1983**, *87*, 640.